On the Implementation of Adaptive Sliding Mode Robust Controller in the Stabilization of Electrically Actuated Micro-Tunable Capacitor

Hamed Mobki, Amin Majidzadeh Sabegh, Aydin Azizi, Hassen M. Ouakad

Abstract:

Parallel-plates based micro-tunable capacitors are known to have low travel range, which worsen as going even lower in terms of their initials gap sizes. Such conditions have put strict requirements on the operation of such designs and hence hindering their use in numerous practical applications requiring high tunability. This work is proposed to examine the possibility to implement a closed-loop control strategy to increase the maximum capacitance and therefore tunability of micro tunable capacitors. The suggested control strategy is implemented on an electrostatically actuated parallel-plates (one stationary and one movable) based micro-capacitor and had an objective to stabilize the movable electrode when it is close to the fixed one for the sake of maximizing its maximum capacitance and possibly improving its overall tunability. Robustness of the micro-capacitor to the so-called pull-in phenomenon (short-circuit instability) when using the closed loop control scheme is studied. Indeed, an adaptive sliding mode controller is designed to compensate the effects of uncertainty, disturbance and eliminate any possibility for chattering phenomenon. The controller proficiencies in terms of stabilizing the micro-capacitor and its robustness to uncertainty as well as disturbance have been thoroughly examined. Furthermore, the effects of the control parameters on the behavior of micro-capacitor, such as overshoot, settling time, steady state error, robustness to uncertainty, external disturbances and to the chattering phenomenon, have been completely inspected. The obtained results indicated satisfactory proficiency and trustworthiness of the proposed control strategy to achieve high level of tunability and maximum capacitance.

Keywords: *micro tunable capacitor, tunability, capacitance, sliding mode control, uncertainty*

1. Introduction

Micro-tunable capacitors are miniature micro-sized structures that find various applications ranging from wireless systems to even high frequency-based circuits. They have attracted the attention of several researchers resulting into the publication of a significant research work [1-5] mainly devoted into considering these tiny structures in the design of numerous devices such as voltage control micro-oscillators [6, 7], micro-filters [8-10], super-heterodyne micro-transceivers [11], etc…

Tunability represents one of most important characteristics for micro-tunable capacitors, which is mainly be governed by the difference between their respective maximum and minimum capacitance values. The more the maximum capacitance is accomplished, the higher the tunability is. Microelectromechanical (MEM) parallel-plates based micro-capacitors have been widely used

in communication transceivers [5] owning high tunability because of numerous reasons: the ease of implementation as simple tuning mechanisms, their low area consumption, their high quality factor and straightforwardness in their fabrication. Indeed, there are three major techniques to possibly increase the tunability of parallel-plates micro-capacitors:

✓ Regulation of the electrodes initial gap distance [12-14],
✓ Optimization of the effective actuated parallel-plates area [15, 16], and
✓ the dielectric displacement method [5, 17].

The above techniques are not commonly successful in increasing the overall maximum capacitance or even in reducing the minimum capacitance to certain optimized levels mainly due to the presence of the pull-in phenomenon (short-circuit instability) in electrostatically actuated parallel-plates based micro-capacitors [18, 19]. Therefore, for such case, modifications are principally made on the mechanical structure of the micro-capacitors [20-25]. Most of these modifications are essentially implemented to withstand the pull-in instability but in most cases, these revisited designs complicate their fabrication processes and cost, create residual stress, and therefore may reduce the overall system reliability [23]. Furthermore, the existence of uncertainty in the fabrication and characterization of MEM devices in addition to the presence of noise/disturbance represent major contributors in reducing the performance of such micro-sized devices [26].

Attracted by the above observations, the utilization of closed loop control strategies to reduce and even compensate the effects of uncertainties and disturbances for the characterization of MEM devices have shown to be successful in increasing their efficiency [27-33]. Moreover, considering the importance of micro-tunable capacitors, several works [27-31] proposed numerous closed-loop control strategies to improve their efficiency and possibly increase their tunability and tuning ratio. An original way to increase the tunability for parallel-plates based capacitor is through using a nonlinear controller to operate its movable electrode very close to its lower stationary actuating electrode without experiencing the pull-in instability. Such scenario results into a drastic increase in the maximum capacitance and therefore increase in the capacitor tunability. But it is worth mentioning that the above control strategy is very challenging and somehow practically impossible as the applied voltage difference assumed between both movable and stationary electrodes depends a lot on the position and the velocity of the movable electrode in addition to the design uncertainties and external perturbations. The sliding mode strategy, which has been considerably considered in

controlling numerous nonlinear systems [34-40], represents an efficient control process that is somehow robust to uncertainties and external disturbances.

This work focuses on designing an adaptive sliding mode controller, derived based on the "Lyapunov" theory, to possibly compensate the effects of uncertainty, disturbance, chattering and control of the pull-in instability in parallel-plates MEM based capacitors. This work aims to reveal the richness and proficiency of the suggested controller in increasing the capacitor tunability as well as maximizing its overall maximum capacitance will been analyzed in the presence of uncertainties and disturbances. Moreover, alterations of the control parameter (the applied voltage) and the effect of the control parameters on the micro-system behavior will be examined. To this end, this research manuscript is organized as follows: Next section overviews the theoretical model used to design the adaptive sliding mode controller. Section 3 summarizes the electro-mechanical model adopted to capture the dynamic behavior of a parallel-plates based micro-sized capacitor. The dynamic behavior of the un-controlled and controlled MEM capacitor is first solved and then discussed in Section 4. Finally, Section 5 presents the summary of concluding remarks of the results for this work.

2. Adaptive Sliding Mode Control Strategy:

In this section, an extended design of the sliding mode controller is suggested based on a former control approach proposed by Aghababa and Akbari [41]. Indeed, in theory work [41] they have presented a methodology to design an adaptive sliding controller to mitigate unwanted high responses in nonlinear systems. For controlling such systems, an independent input needs to be controlled at each state and at a given error. They considered a sliding surface to be governed by the following state equation: $s = \lambda e$: where the parameter s represents the sliding surface, e represents the error and λ symbolizes a positive number. Knowing that the dynamic equation of a parallel-plates based capacitor has someway differences with the dynamic nonlinear system presented in [41], their methodology cannot be applied accordingly without few revisions. Therefore, we intend next to extend the method described in reference [41] to design an adaptive sliding mode controller for the following state-space dynamical system:

$$\begin{cases} \dot{x}_1 = x_2 \\ \dot{x}_2 = f(x,t) + g(x,t)u + d(t) + \Delta F(x,t) \end{cases} \tag{1}$$

where: x, u, and t represent respectively the state, input, and time variables. The parameter $f(x,t)$ and $g(x,t)$ are non-linear functions, that satisfy the Lipchitz condition [42]. The functions $\Delta F(x,t)$ and $d(t)$ denote both the uncertainty and disturbance conditions. For the case of the dynamical system governed by Eq. (1), the following design conditions: $|\Delta F(x,t)| \leq \alpha$ and $|d(t)| \leq \beta$ where α and β are both positive values, are considered. If the purpose of the designed control is to track a desired path of x_d for the dynamical variable $x_1(t)$, the system dynamic error can be defined as $e_1 = x_1 - x_d$. The considered controller is intended to force the dynamic response wave $x_1(t)$ to follow a desired wave x_d, or, in other words, to make sure the system dynamic error e_1 wave converges to a small value. Considering this definition and assuming that the dynamic error will be governed by the following system of equations:

$$\begin{cases} \dot{e}_1 = e_2 \\ \dot{e}_2 = f(x,t) + g(x,t)u + d(t) + \Delta F(x,t) - \ddot{x}_d \end{cases} \tag{2}$$

Since, there is not any independent input to control the dynamic error wave e_1, thus, unlike what is suggested in reference [41], the sliding surface for this work will be considered to mimic the following equation: $s = \dot{e}_1 + k_s e_1$, where k_s is a positive number. Actually, this choice is intended not only to control and stabilize the error wave e_1, but also to guarantee the controller's stability and the convergence of the dynamic response wave to the desired path x_d. In addition, if the input wave function u is defined as in the below Eq. (3), the controller's stability will be guaranteed and the dynamic response convergence will be also assured (proof of stability in Appendix A).

$$u = -\frac{1}{g(x,t)}\left[f(x,t) - \ddot{x}_d + k_s e_2 + \left(\hat{\alpha} + \hat{\beta} + \mu\right)\tanh(\theta s)\right] \tag{3}$$

where $\hat{\alpha} > 0$ and $\hat{\beta} > 0$ are two positive adaptive parameters used for the adaptation of the uncertainty and disturbance functions, respectively. The parameters $\mu > 0$ and $\theta > 0$ are similarly two positive adaptation coefficients to tune the system gain and the abruptness of the "*tanh*" function, respectively. The previously mentioned adaptation parameters are updated using the following adaptive laws:

$$\dot{\hat{\alpha}} = -|s| \qquad \hat{\alpha}(t=0) = \hat{\alpha}_0 > 0 \qquad (4)$$
$$\dot{\hat{\beta}} = -|s| \qquad \hat{\beta}(t=0) = \hat{\beta}_0 > 0$$
$$\dot{\mu} = -p|s||e_1| \qquad \mu(t=0) = \mu_0 > 0$$
$$\dot{\theta} = -q|s||e_1| \qquad \theta(t=0) = \theta_0 > 0$$

where p and q are both positive values, and the values $\hat{\alpha}_0$, $\hat{\beta}_0$, μ_0, and θ_0 represent initial values for updating the parameters of $\hat{\alpha}$, $\hat{\beta}$, μ, and θ.

3. Parallel-Plates Micro Capacitor Electro-Mechanical Model:

In this section, the electro-mechanical model of a micro-sized parallel-plates based capacitor is overviewed. The top-view microscopy image and a side-view simple 2D schematic view of the considered capacitor are both shown in Fig. 1a and 1b, respectively. In the simple 2D schematic of Fig. 1b, the movable (upper) and fixed (lower) electrode are displayed. Figure 1a represents the top view of micro capacitor where it shows the upper movable electrode. The initial gap distance between the upper and lower electrodes is symbolized as G_0 and V denotes the applied voltage between both electrodes. The applied voltage causes an attractive force that pushes the moving electrode toward the stationary resulting into a reduction of the initial gap distance between the two electrodes. This decrease of the initial distance increases according the capacitance and, consequently, increases the micro-capacitor tunability.
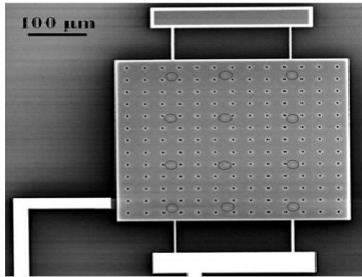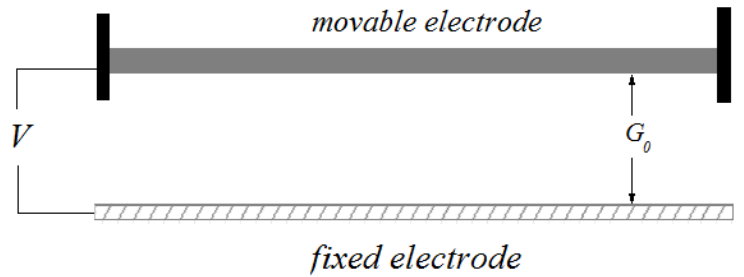
(a) Top-View [43]   (b) Side-View

Fig. 1. (a) Top-View and (b) Side-View Schematics of a tunable parallel-plates based capacitor.

As shown in the top-view of Fig. 1a, the movable electrode is suspended with four thin arms. Consequently, the overall equivalent stiffness of the suspended electrode system is $k_{eq} = 4 \times k_{arm}$.

Each arm stiffness is equal to $k_{arm} = 12EI/L^3$, where E, $I = bh^3/12$, and L represent the Young's modulus of elasticity, the cross-sectional moment of inertia, and the arm length, respectively, and b and h are both the width and thickness of each arm, correspondingly. For simplicity, we assumed that the thickness of all four arms is the same as the thickness of the movable electrode and all are made of homogeneous material with mass density ρ.

The governing dynamic equation of the moving electrode without considering uncertainties and external disturbances can be simply written as follows:

$$m\frac{d^2z}{d\tau^2} + c\frac{dz}{d\tau} + k_{eq}z = \frac{\varepsilon_0 AV^2}{2(G_0 - z)^2} \tag{5}$$

where m, c, and A represent mass, damping coefficient, and the cross-sectional area of the moving electrode, respectively. In the above equation, the forcing term $\varepsilon_0 AV^2/2(G_0 - z)^2$ denotes the attractive electrostatic force between the moving and fixed electrodes where ε_0 symbolizes the permittivity of the vacuum and z indicates the relative displacement of the movable electrode with respect to the fixed one. Considering the following normalizing variables:

$$w = \frac{z}{G_0}, \quad t = \frac{\tau}{t^*}, \quad t^* = \sqrt{\frac{k_{eq}}{m}}, \quad c' = \frac{c}{k_{eq}t^*}, \quad \gamma = \frac{\varepsilon_0 S}{2k_{eq}G_0^3}, \tag{6}$$

Eq. (5) can be simplified in a dimensionless form as follows [43]:

$$\frac{d^2w}{dt^2} + c'\frac{dw}{dt} + w = \frac{\gamma V^2}{(1-w)^2} \tag{7}$$

where t denotes the dimensionless time.

Next, assuming the following state-space variable $w = x_1$ and $\dot{w} = \dot{x}_1 = x_2$, and considering the presence of uncertainties and external disturbances designated by the following functions: $\Delta F(x,t)$ and $d(t)$, respectively, Eq. (7) can be re-written in a state-space form as follows:

$$\begin{cases} \dot{x}_1 = x_2 \\ \dot{x}_2 = -x_1 - c'x_2 + \dfrac{\gamma V^2}{(1-w)^2} + \Delta F(x,t) + d(t) \end{cases} \qquad (8)$$

The above equations represent the dynamic equation of tunable micro-capacitor in a standard form like the one in Eq. (1) and taking into consideration the uncertainties and disturbances effects. Next, assuming $u = V^2$ to be control parameter, and considering the state error as $e = x_1 - x_d$, the dynamic equation governing the error can be simply derived as follows: $\dot{e} = \dot{x}_1 - \dot{x}_d = x_2 - \dot{x}_d$. Besides, the governing dynamic equation of error can be therefore expressed as:

$$\begin{cases} \dot{e}_1 = e_2 \\ \dot{e}_2 = -x_1 - c'x_2 - \ddot{x}_d + \dfrac{\gamma V^2}{(1-w)^2} + \Delta F(x,t) + d(t) \end{cases} \qquad (9)$$

Assuming the above equation, the control law can be obtained easily using eq. (3).

4. Results and discussion:

In this section, the obtained results and relevant discussion will be succinctly presented and discussed. The coming first batch of results are based on neglecting the uncertainties and disturbances. The Physical and geometric properties of the simulated micro-capacitor are summarized in Table 1.

Table 1. Physical and geometric properties of the micro tunable micro-capacitor.

Properties	Value
Area of movable electrode (S)	$400\,\mu m \times 400\,\mu m$
Thickness of each arm (h)	$2\,\mu m$
Thickness of movable electrode (h)	$2\,\mu m$
Length of each arm (L)	$200\,\mu m$
Width of each arm (b)	$5\,\mu m$
young's modulus (E)	$169GPa$
Initial gap size (G_0)	$3\,\mu m$
Mass-density (ρ)	$2300\,{kg}/{m^3}$

4.1. Control of micro tunable capacitor without considering of uncertainties and disturbances

As a first case, we consider the case of $x_d = 0.95$, and the control parameters were all assumed as follows: $k_s = 0.1$, $\mu_0 = 5$, $\theta_0 = 50$, $q = 1$, and $p = 1$. The results of Fig. 2 are only for demonstration purpose and only to show the capability of the controller to regulate the dynamic response of the micro capacitor. Figures 2a-2g show the time history variations of the micro-capacitor displacement, the system dynamic error, the micro-system capacitance, the applied voltage, as well as the variations of the adaptation coefficients (θ and μ), respectively for a tracking value of $x_d = 0.95$. As shown in Figs. 2a and 2b, the movable electrode is exactly placed at distance of $0.05 \mu m$ from the fixed electrode and the corresponding dynamic error converges to zero at the steady-state. In addition, Fig. 2c shows the maximum capacitance of the micro-capacitor reaching a value of $\approx 9.44 \times 10^{-12} F$. Given the fact that the calculated minimum capacitance for this case is around $\approx 47.22 \times 10^{-14} F$ and using the following relationships to compute the respective values of the capacitor tunability and tuning ratio as follows: $\text{Tunability} = \dfrac{C_{max} - C_{min}}{C_{min}} \times 100\%$ and

$\text{Tuning\_Ratio} = \dfrac{C_{max}}{C_{min}} \times 100\%$, they were both found to be equal to 1900% and 2000%, respectively, demonstrating significant values. The minimum capacitance for this micro capacitor is fixed and it is equal with $47.22 \times 10^{-14} F$ but with the help of presented method the minimum gap between two electrodes can reach to $0.05 \mu m$ and consequently the maximum capacitance can reach to value of $9.44 \times 10^{-12} F$. The micro-capacitor voltage time-history variation is presented in both Figs. 2d and 2e. As shown in Fig. 2e, the applied voltage starts to decrease from ≈ 25.3 *Volt* reaching zero around $\tau \approx 2.97 \times 10^{-6} s$, then around $\tau \approx 2.42 \times 10^{-5} s$ it starts again to increase reaching a value of ≈ 1 *Volt* to then smoothly decreases again and remains equal to ≈ 0.5 *Volt* at the steady-state. Moreover, the time-history variations of the adaptations coefficients θ and μ are shown in both Figs. 2f and 2g, respectively. As it is evident from the obtained curves, both parameters decrease with time and when reaching $\tau \approx 2.34 \times 10^{-5} s$ they both attain their respective steady-state values denotes by: $\theta_{ss} \approx 49.87$ and $\mu_{ss} \approx 4.87$. As seen from all the results of Figure 2, with the advantage of the controller, the micro-capacitor was able to track the mentioned path with relatively acceptable proficiency. But it is worth mentioning here that because we considered in this case, the distance between the two electrodes to be considerably small, the effects of

dispersion forces such as the Van der Waals and Casimir forces can be reasonably noticeable and such disturbing forces may cause to premature dynamic pull-in instability. These forces are often not considered in the mathematical modeling of micro-systems, but these forces are considered in the modeling of nanostructures and play an important role in the dynamical behavior of nanostructures.

In addition, any overshoot in the response of the micro-capacitor may cause as a premature dynamic pull-in as well. In the rest of this section, it will be shown that changing any of the controller parameters may cause an overshoot in the system response. Therefore, and in order to avoid any pull-in phenomenon, in the rest of this investigation the desired path will be restricted to values not exceeding 0.9.
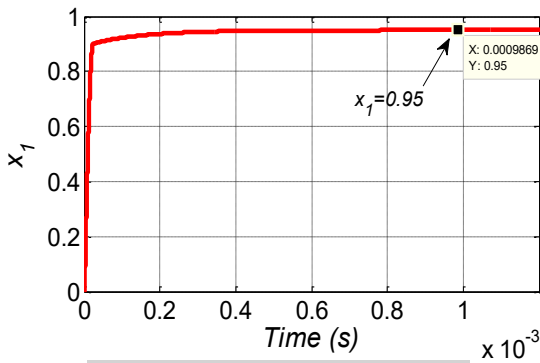
Fig. 2a) variation of x_1 versus time
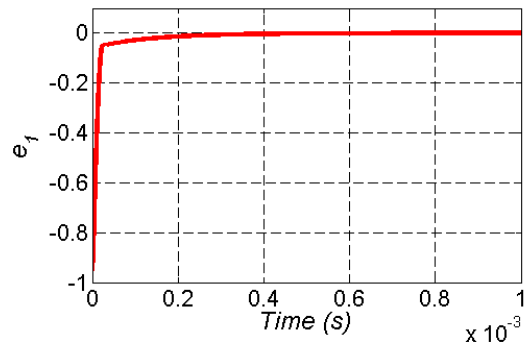
Fig. 2b) variation of e_1 versus time
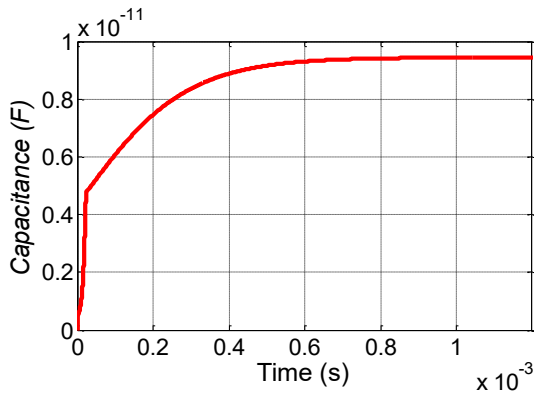
Fig. 2c) variation of C versus time
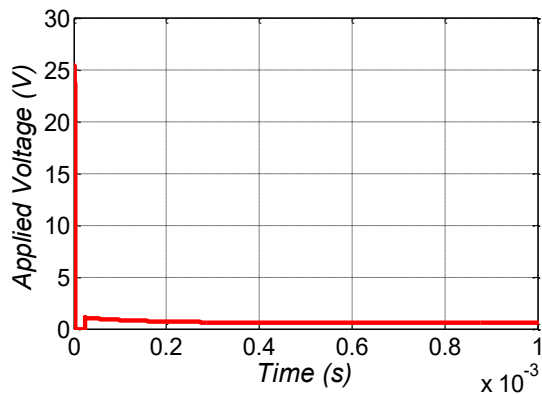
Fig. 2d) variation of V versus time
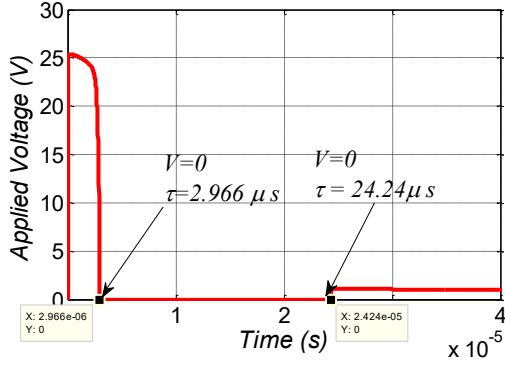
Fig. 2e) Zoomed view of Fig 1d
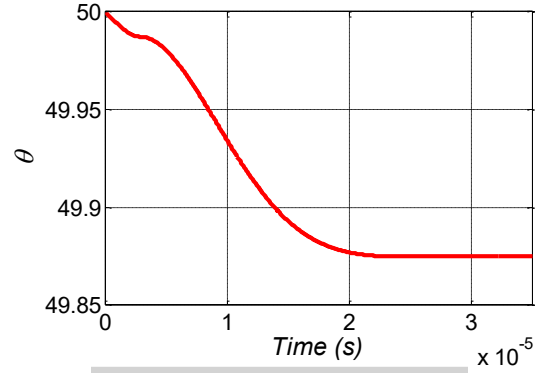
Fig. 2 f) variation of θ versus time
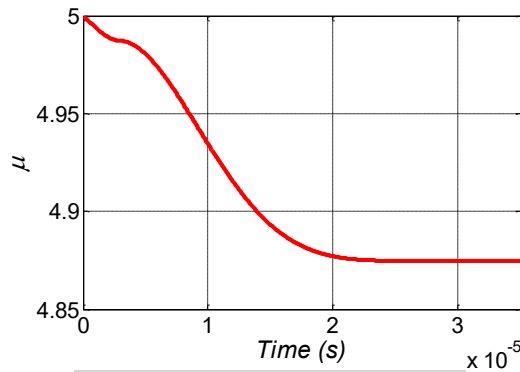
Fig. 2 g) variation of μ versus time

Fig. 2) obtained result for control of the micro tunable capacitor considering $x_d = 0.95$

The relevant results of x_1, e_1, c, V for the tracking of the different values of x_d are shown in Figs 3a-3e. As demonstrated by Figs. 3a and 3b, an overshoot is observed in the behavior of x_1 and e_1, but for higher values of x_d, the level of overshoot significantly decreases. Such overshoot can also be seen in the variation of capacitance. The amount of applied voltage versus time is also shown in Figures 3d and 3e. For the time interval of $3 \times 10^{-6} s \leq \tau \leq 2.4 \times 10^{-5} s$, the voltage level reaches zero. As exposed in Fig. 3d, the initial voltage level for all x_d except $x_d = 0.2$ is about $25\ V$ and as time elapses, it reaches zero. By increasing x_d the amount of applied voltage, reaches zero at higher time. Also, according to Fig. 3e, for $\tau \geq 2.4 \times 10^{-5} s$ and smaller x_d, more voltage is needed and this voltage reaches its peak at a later time.
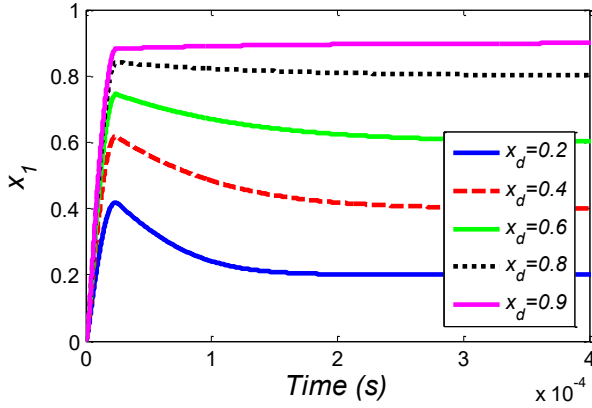
Fig. 3a) variation of x_1 versus time for different values of x_d
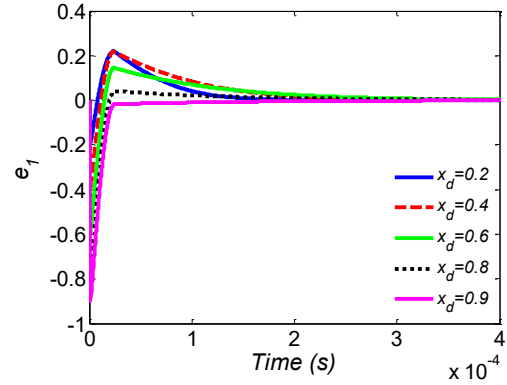
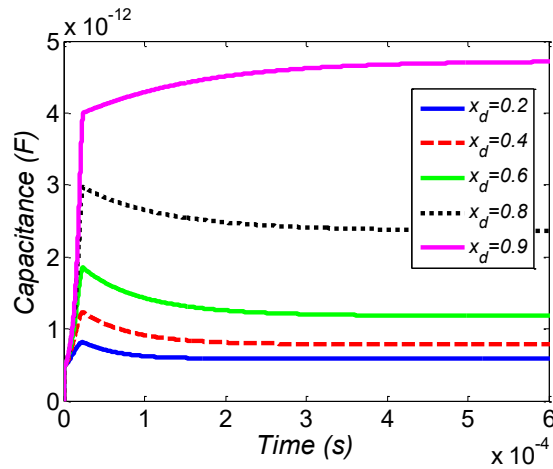Fig. 3b) variation of e_1 versus time for different values of x_d

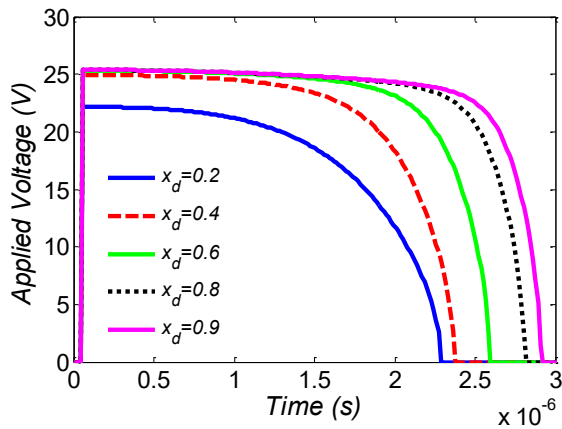Fig. 3c) variation of C versus time for different values of x_d

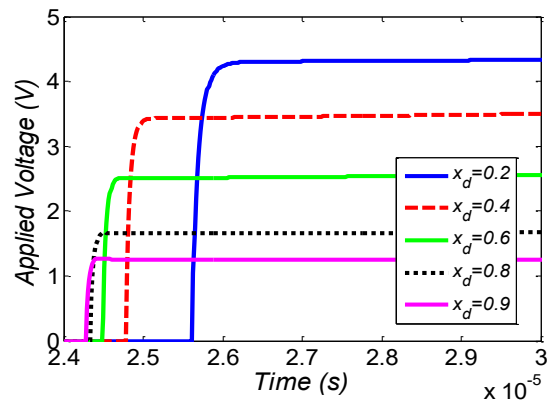Fig. 3d) variation of V versus time ($0 \leq \tau \leq 3 \times 10^{-6} s$) for different values of x_d

Fig. 3e) variation of V versus time ($2.4 \times 10^{-5} \leq \tau \leq 3 \times 10^{-5} s$) for different values of x_d

Fig. 3) The relevant results of x_1, e_1, c, V for tracking of different values of x_d

The maximum capacitance, tunability as well as tunning ratio for different values of x_d are summarized in Table 2. As it is clear from the table that a relatively high value of tunability is reachable by means of active control as well as utilization of proposed adaptive sliding mode controller.

Table 2. The acquired level of maximum capacitance, tunability, as well as tunning ratio for different values of x_d by application of proposed controller ($C_{\min} = 4.72 \times 10^{-13} F$)

	$x_d = 0.2$	$x_d = 0.4$	$x_d = 0.6$	$x_d = 0.8$	$x_d = 0.9$
$C_{\max}$ (F)	5.90×10^{-13}	7.87×10^{-13}	11.81×10^{-13}	23.66×10^{-13}	47.10×10^{-13}
tunability	25.01%	66.69%	150.11%	401.06%	897.45%
tunning ratio	125.01%	166.69%	250.11%	501.06%	997.45%

In the following, we propose to examine the behavior of the system for different values of k_s, μ, and θ. Variations of e_1, C, and V have been plotted in figs. 4a to 4d for $x_d = 0.2$ and different values of k_s. As shown in Fig. 4a, the overshoot level increases significantly with increase of k_s, but the error converges to zero, in less time. But as shown in this figure, settling times are in the order of $0.5 \times 10^{-4} s$ and $1.5 \times 10^{-4} s$ for $k_s = 1$ and $k_s = 0.1$, which are both very small magnitude and for $k_s = 0.1$ capacitor has a enough quick response; so, for this case, overshoot should be considered $k_s = 0.1$ or $k_s = 0.2$. It is worth noting that an assumed higher overshoot increases the collision possibility between two electrodes, as is apparent from this figure, for $k_s = 1$ a movable electrode is at the threshold of contact with the fixed electrode.

Similarly, time dependent capacitance changes are shown in Fig. 4b. As can be seen from this figure, the overshoot level for capacitance is higher than the overshoot generated in the error of e_1, and it shows the more sensitivity of capacitance to k_s. In addition, the values of applied voltage

are plotted in Figures 4c and 4d. As it can be seen, the initial applied voltage is about 25 V for $k_s \geq 0.2$, but for $\tau \geq 15 \times 10^{-5} s$, this value is the same for all modes.
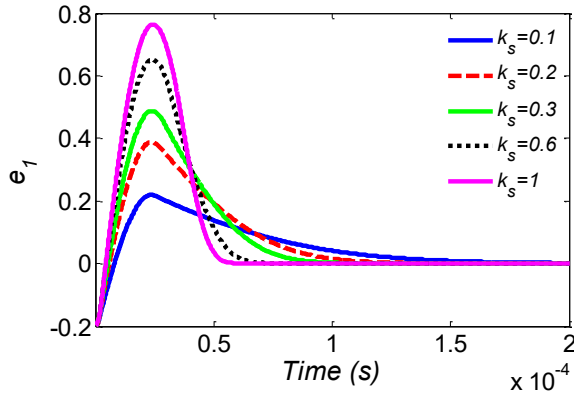

Fig. 4a) variation of e_1 versus time for different values of k_s and $x_d = 0.2$
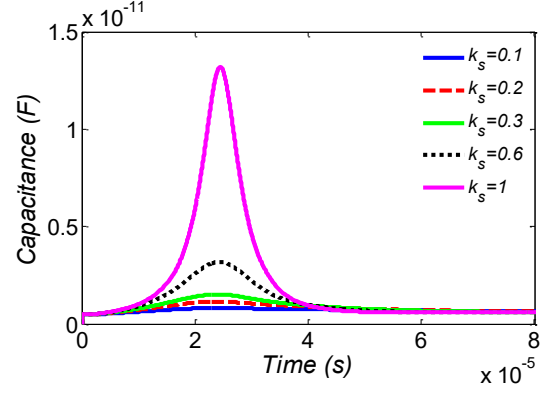
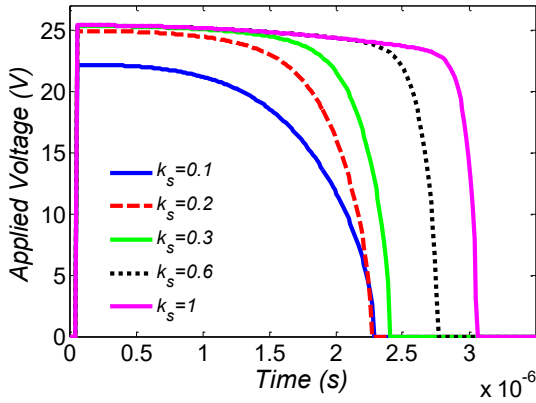Fig. 4b) variation of C versus time for different values of k_s and $x_d = 0.2$

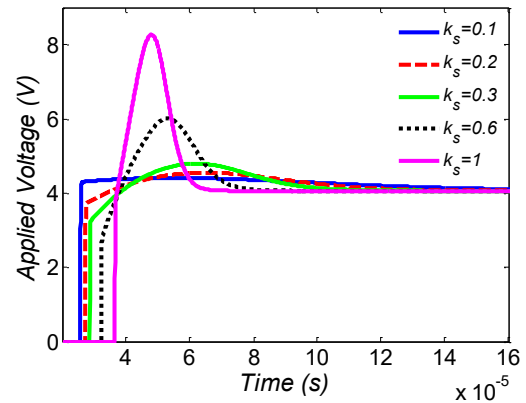Fig. 4c) variation of V versus time ($0 \leq \tau \leq 3.5 \times 10^{-6} s$) for different values of k_s and $x_d = 0.2$

Fig. 4d) variation of V versus time ($2 \times 10^{-5} s \leq \tau \leq 16 \times 10^{-5} s$) for different values of k_s and $x_d = 0.2$

Fig. 4) The relevant results of x_1, e_1, c, V for tracking of $x_d = 0.2$ and different values k_s

The results for different values of μ and $x_d = 0.2$ are subsequently plotted in Fig. 5a-5d. As shown in Figs. 5a and 5b, an increase of μ causes an increase of the overshoot, the control error, the capacitance, as well as the system settling time. In addition, according to Fig. 5c, it is clear, that the initial value of voltage increases with the increase of μ, but a relatively higher voltage is reaching zero in shorter time. Additionally, for $\tau \geq 2.5 \times 10^{-4} s$ no significant change in the voltage can be observed, furthermore the voltage level for different μ and $\tau = 3 \times 10^{-4} s$ tends to 4.06 V.

Therefore, given that the increase of μ causes to increase in overshoot and initial voltage, it is suggested to use less value of μ (e.g. $\mu = 1$) in the controller design.
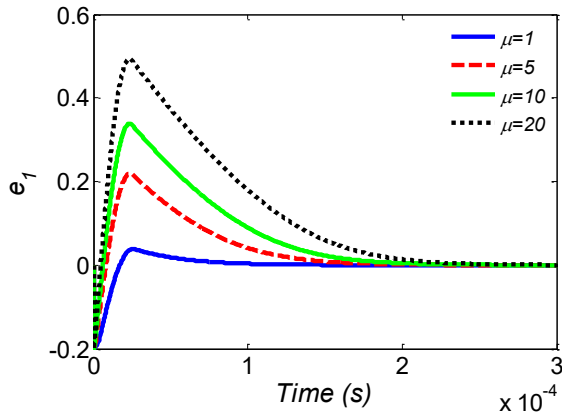

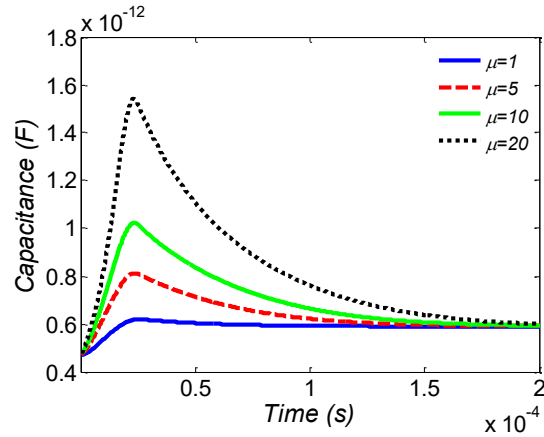Fig. 5a) variation of e_1 versus time for different values of μ and $x_d = 0.2$

Fig. 5b) variation of C versus time for different values of μ and $x_d = 0.2$
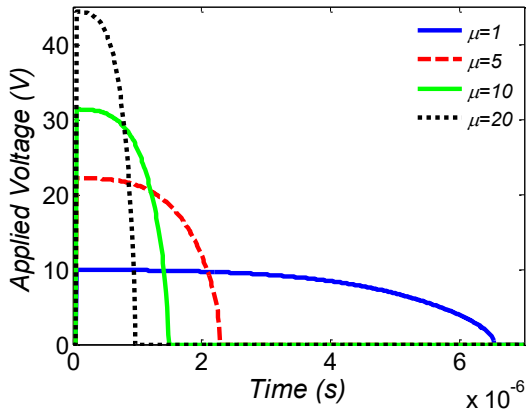
Fig. 5c) variation of V versus time ($0 \le \tau \le 7 \times 10^{-6} s$) for different values of μ and $x_d = 0.2$
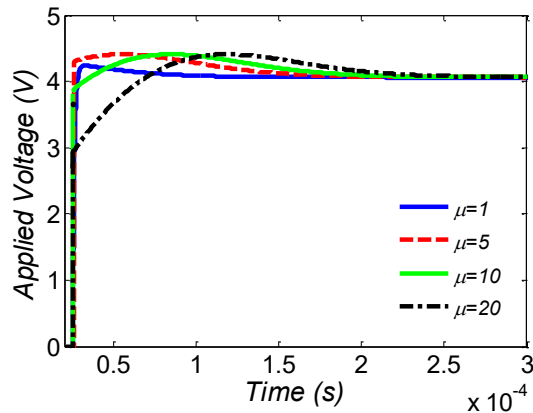
Fig. 5d) variation of V versus time ($2.03 \times 10^{-5} s \le \tau \le 3 \times 10^{-4} s$) for different values of μ and $x_d = 0.2$

Fig. 5) The relevant results of x_1, e_1, c, V for tracking of $x_d = 0.2$ and different values μ

The diagrams of e_1 and the capacitance changes assuming an $x_d = 0.2$ and for different values of θ are presented in Figures 6a and 6b. As seen from these plots, any increase of θ causes systematically an increase of the overshoot, the controller error signal, as well as its capacitance. Moreover, an assumed applied voltage of $\theta = 5000$ is shown in Fig. 6c and 6d. As can be seen from the figures, a chattering phenomenon is formed for the interval of $\tau \ge 2.52 \times 10^{-4} s$. In fact, as θ increases, the approximation of $\tanh(\theta s) = sign(s)$ becomes more accurate and for higher

values of θ there is discontinuity around $s = 0$, which causes a sharp switching at the sliding surface and creates chattering consequently.
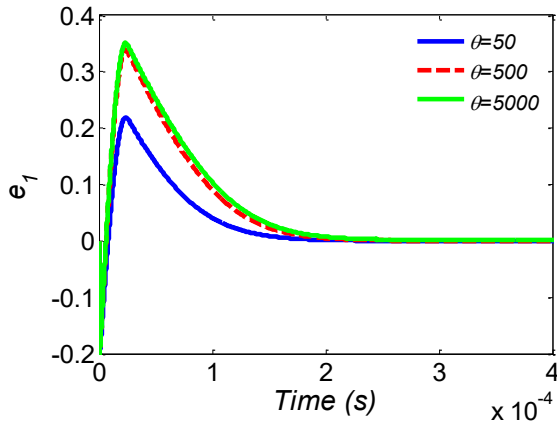

Fig. 6a) variation of e_1 versus time for different values of θ and $x_d = 0.2$
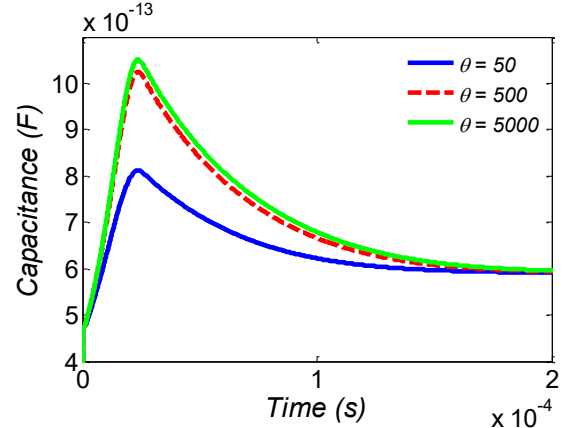

Fig. 6b) variation of C versus time for different values of θ and $x_d = 0.2$
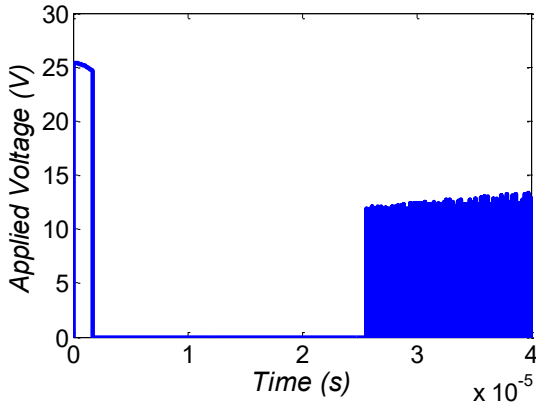

Fig. 6c) variation of V versus time ($0 \le \tau \le 4 \times 10^{-5} s$) for $\theta = 5000$ and $x_d = 0.2$
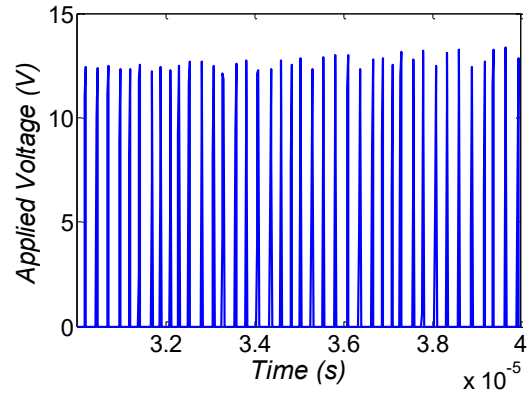

Fig. 6d) detailed view of fig 6c

Fig. 6) The relevant results of e_1, c, V for tracking of $x_d = 0.2$ and different values θ

The capacitance and e_1 diagrams are demonstrated in Figures 7 and 8 assuming $x_d = 0.6$ and $x_d = 0.9$. The figures show that an increase in θ in addition to an increase of the overshoot causes consequently an apparition of a steady state error in the system. In addition, for higher values of an assumed x_d, the level of the steady state error becomes more noticeable. Therefore, for higher values of θ and of the overshoot, a steady state error is created and therefore increases the

probability of occurrence of the chattering phenomenon. For this, it is suggested to use the following value of $\theta = 50$.
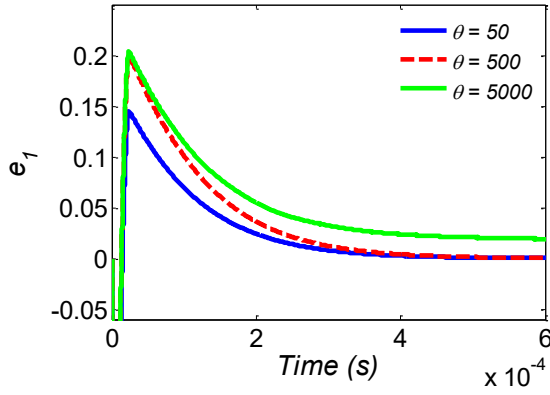

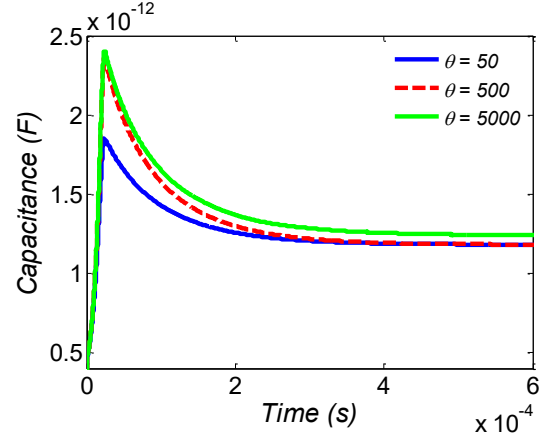Fig. 7a) variation of e_1 versus time for different values of θ and $x_d = 0.6$

Fig. 7b) variation of C versus time for different values of θ and $x_d = 0.6$

Fig. 7) The relevant results of e_1 and C for tracking of $x_d = 0.6$ and different values θ
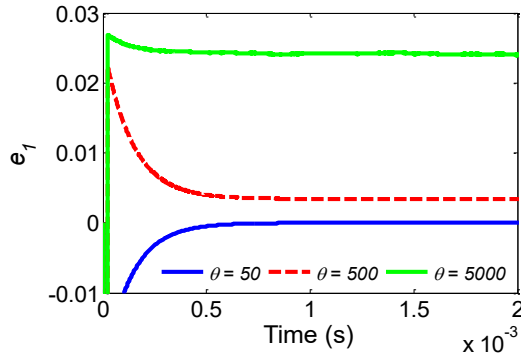

Fig. 8a) variation of e_1 versus time for different values of θ and $x_d = 0.9$
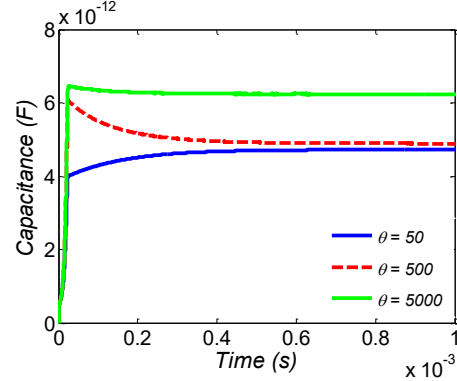
Fig. 8b) variation of C versus time for different values of θ and $x_d = 0.9$

Fig. 8) The relevant results of e_1 and C for tracking of $x_d = 0.9$ and different values θ

4.2. Robustness assessment of controller in the presence uncertainties and disturbances

As a continuation of this investigation, the robustness of the suggested controller to uncertainties and disturbances will be subsequently investigated. For this case, the terms of uncertainty and disturbance are considered as $\Delta F(x,t) = \alpha \gamma \sin(x_1)$ and $d(t) = \beta \gamma \sin(t)$, respectively.

Figures 9a and 9b show diagrams of e_1 and capacitance for different values of α, $\beta = 5$ and $x_d = 0.2$. As these forms show, with increasing α or level of uncertainty, overshoot and settling time increase. The voltage variation for this case is also plotted in Figures 9c and 9d.

As already mentioned earlier, any decrease in k_s and μ reduces the overshoot consequently. The diagram of e_1 and capacitance variation for $\alpha = 100$, $\beta = 5$, and $x_d = 0.2$, and for different values of k_s and μ are the presented in Fig. 10a and 10b. As shown in these Figures, decreasing k_s and μ, reduces the overshoot. The voltage variation diagrams for these particular cases are also shown in Fig. 10c.

Fig. 9a) variation of e_1 versus time for different values of α, $\beta = 5$ and $x_d = 0.2$

Fig. 9b) variation of C versus time for different values of α, $\beta = 5$ and $x_d = 0.2$

Fig. 9c) variation of V versus time ($0 \leq \tau \leq 2.5 \times 10^{-6} s$) for for different values of α, $\beta = 5$ and $x_d = 0.2$

Fig. 9d) variation of V versus time ($2.2 \times 10^{-5} s \leq \tau \leq 7 \times 10^{-4} s$) for for different values of α, $\beta = 5$ and $x_d = 0.2$

Fig. 9) The relevant results of e_1, c, V for tracking of $x_d = 0.2$ and different values of α and $\beta = 5$
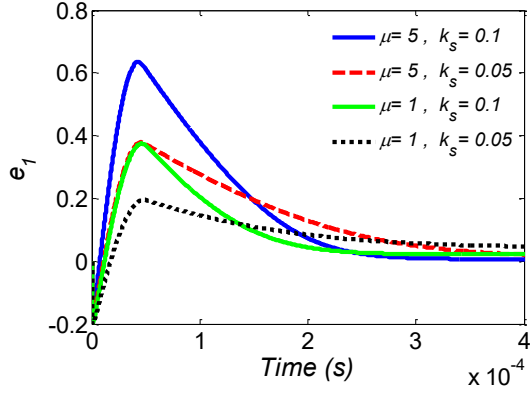
Fig. 10a) variation of e_1 versus time for different values of k_s and μ , $\alpha = 100$, $\beta = 5$ and $x_d = 0.2$
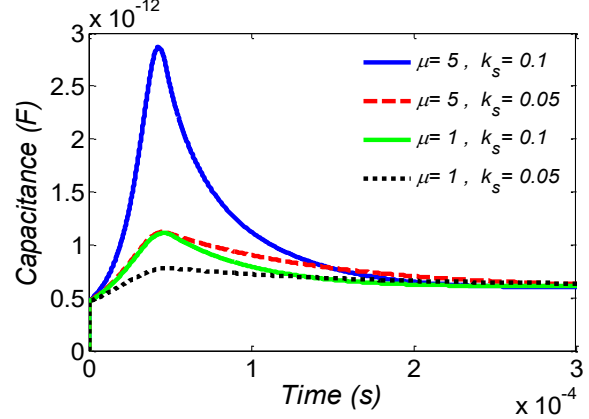
Fig. 10b) variation of C versus time for different values of k_s and μ , $\alpha = 100$, $\beta = 5$ and $x_d = 0.2$
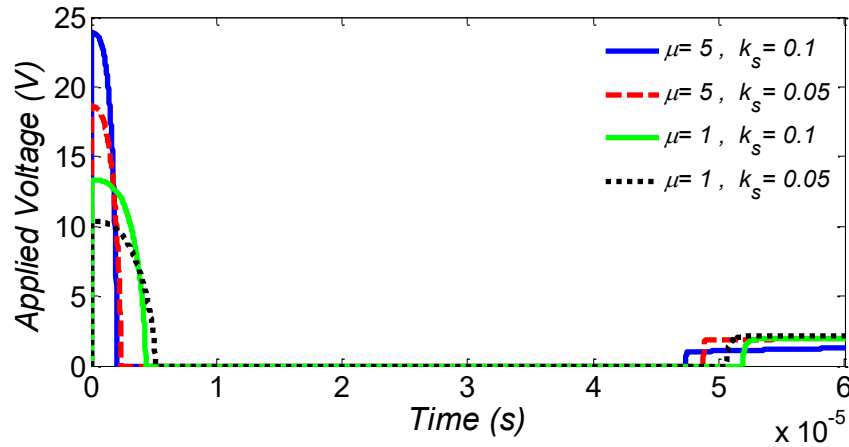
Fig. 10c) variation of V versus time for different values of k_s and μ , $\alpha = 100$, $\beta = 5$ and $x_d = 0.2$

Fig. 10) The relevant results of e_1 , C , and V for tracking of $x_d = 0.2$, $\alpha = 100$ and $\beta = 5$ and different values of μ and k_s

Next, the diagrams of e_1 and capacitance for $\alpha = 5$, $x_d = 0.2$, and different values of β are plotted in Figures 11a and 11b. As it is demonstrated by these figures, with a relative increase in β results intyo an increase in both the overshoot, and the settling time. Nevertheless, any increase of β has a significant impact on the settling time. To more elucidate on this, an assumed voltage variation for different β are depicted in Fig. 11c. As it is noticeable from this sketch the presence of noise causes oscillations of the applied voltage for $\tau \geq 2.5 \times 10^{-5} s$, which fluctuations are to compensate the noise effects.
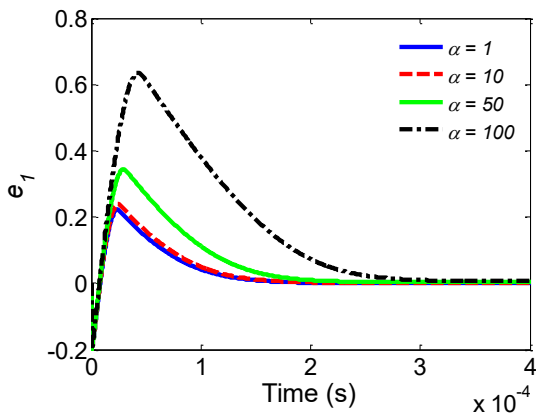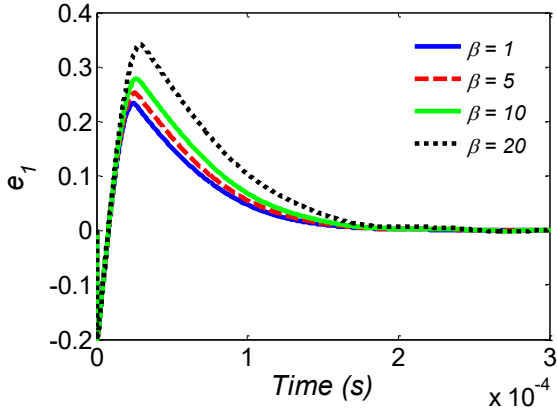
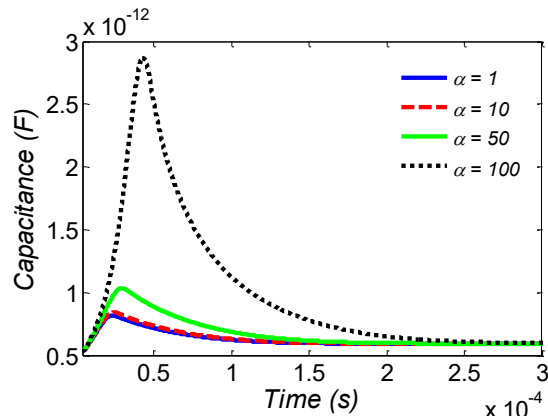Fig. 11a) variation of e_1 versus time for different values of β , $\alpha = 5$ and $x_d = 0.2$
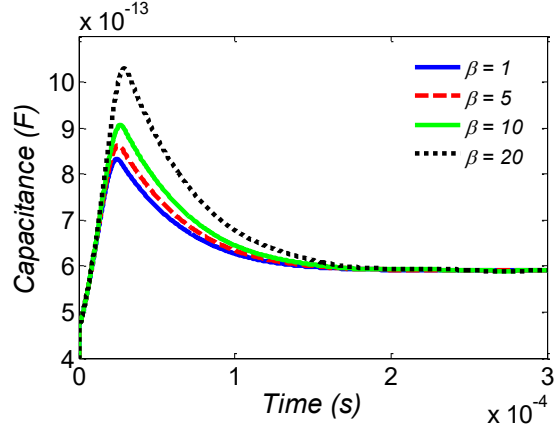
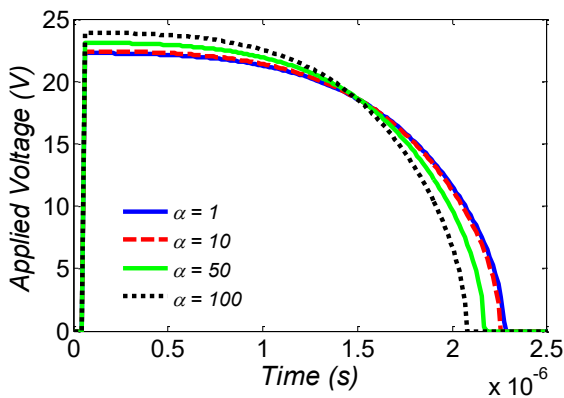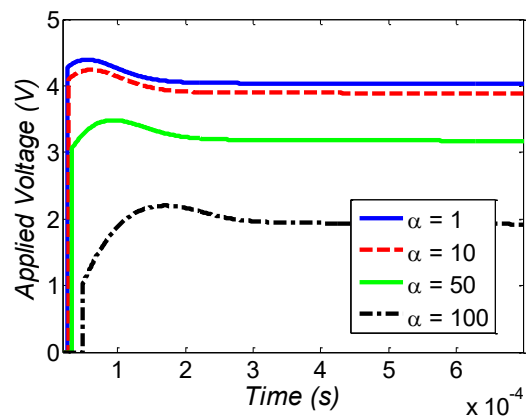Fig. 11b) variation of C versus time for different values of β , $\alpha = 5$ and $x_d = 0.2$
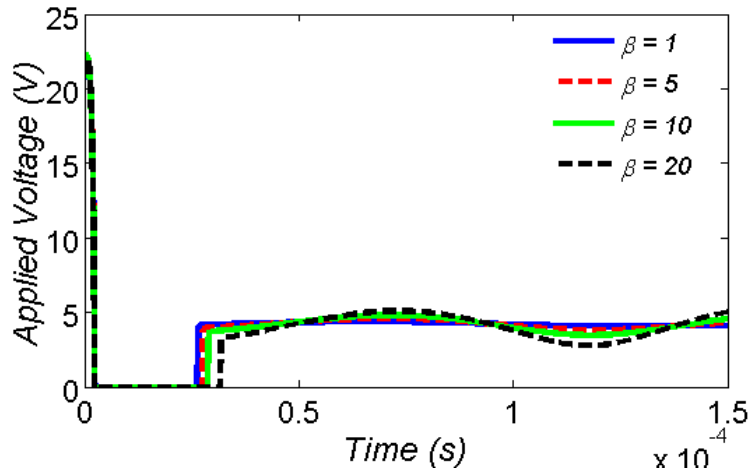
Fig. 11c) variation of V versus time for for different values of β , $\alpha = 5$ and $x_d = 0.2$

Fig. 11) The relevant results of e_1, C, and V for tracking of $x_d = 0.2$ and different values of β and $\alpha = 5$

Changes of e_1 together with capacitance variation for $\beta = 20$ and different values of μ and k_s are shown in Figs. 12a and 12b. It is clear from these figures that decreasing both μ and k_s reduces consequently the overshoot level. Additionally, the variations of applied voltage versus time are plotted in Fig. 12c. As it is evident from these variations that an assumed increase of μ causes a rise of the initial value of applied voltage.
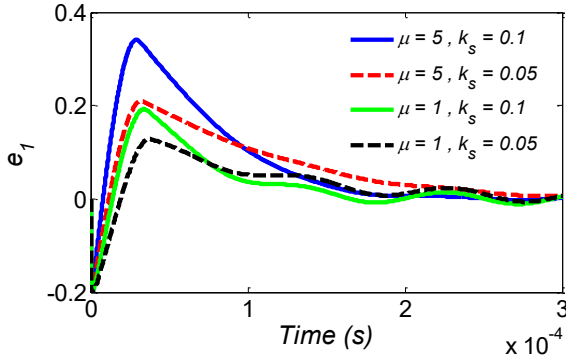
Fig. 12a) variation of e_1 versus time for $\beta = 20$, $\alpha = 5$ and $x_d = 0.2$ and different values of k_s and μ
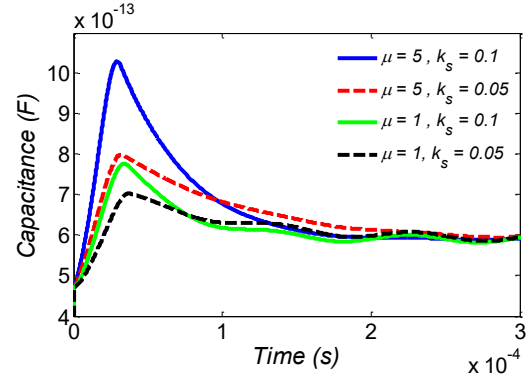
Fig. 12b) variation of C versus time for $\beta = 20$, $\alpha = 5$ and $x_d = 0.2$ and different values of k_s and μ
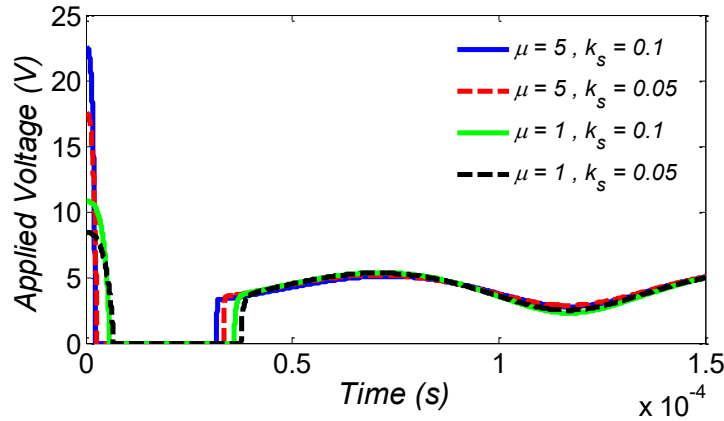
Fig. 12c) variation of V versus time for $\beta = 20$, $\alpha = 5$ and $x_d = 0.2$ and different values of k_s and μ

Fig. 12) The relevant results of e_1, C, and V for tracking of $x_d = 0.2$, $\alpha = 5$ and $\beta = 20$ and different values of μ and k_s

At the end of this sub-section, some of the achieved results related to improvement of tunability in recent years are summarized in Table 3. The examined processes in the cited works in Table 3 were carried out without the utilization of an active control strategy, and were all based on restructuring of capacitance to increase the secondary stiffness, increase the maximum capacitance, and/or reduce the minimum capacitance. In fact, and after a thorough look at the current literature, the authors haven't found any single research work related to the tenability improvement using an active control strategy. It is important to note that in these cited research works in Table 3, the proposed structures were more complex than the assumed conventional parallel plate capacitors in our work, which makes it very difficult to be fabricated. Comparison of the presented results of this work with the other research outcomes summarized in Table 3

shows the remarkable capability of the presented control strategy in increasing the micro-capacitor tunability as well as tuning ratio. In addition, the obtained results in this work show the high reliability of the micro-capacitor to uncertainties and perturbations.

Table 3. Achieved results related to improvement of tunability of micro tunable capacitors in recent years

	Maximum tunability	Maximum tuning range	Capacitor type
Akhtar et al. 2018 [21]	168%	268%	Parallel plate
Hailu 2017 [44]	-	143%	Comb drive
Kim et al. 2017 [45]	414%	514%	Parallel plate
Afrang et al 2015 [46]	207%	307%	Parallel plate
Mobki et al 2014 [47]	147%	247%	Parallel plate
Shavezipur 2012 [48]	157%	257%	Parallel plate
Mobki et al 2011 [49]	100%	200%	Parallel plate
Shavezipur et al 2010 [50]	152%	252%	Parallel plate

5. Conclusion

In this work, an adaptive sliding mode controller was proposed and investigated to control a parallel-plates based tunable micro-capacitor. The purpose of the capacitor control is to track the movable electrode to close distance to its lower fixed actuating electrode in order to increase its overall maximum capacitance $C_{\max}$ and therefore its tunability. The obtained results indicated the substantial capability of this control strategy in increasing the maximum capacitance $C_{\max}$ and the capacitor tunability. In addition, the adaptive sliding mode controller was examined to mitigate the effects of uncertainties, external disturbances as well as to possibly eliminate any chattering phenomenon. Furthermore, it was shown that the controller possesses high robustness to compensate the uncertainties and disturbances effects.

The effects of controller parameters on the dynamic behavior of the micro-capacitor were completely examined. The results showed that any increase of the controller positive gain coefficient k_s as well as controller adaption positive coefficient μ resulted into a rise in the micro-capacitor overshoot level as well as its settling time. Moreover, it was shown that the micro-capacitor overshoot level decrease with the decrease of the controller adaptation positive parameter θ. Indeed, it was found that chattering phenomenon can be observed when the adaptation coefficient θ reaches a value around ≈ 5000 and that any increase of this coefficient can cause the

stabilization in both the steady-state dynamic error e_1 and the micro-capacitor overall capacitance. Finally, it was found that, in the presence of uncertainties and external disturbances causing an definite increase in the micro-system dynamic response overshoot and in order to reduce it to an acceptable range, it is suggested to consider both positive controller coefficients k_s and μ to be both small values.

Appendices:

Appendix A: Proof of the controller stability

If we consider a Lyapunov function described by the below expression:

$$v = \frac{1}{2}\left[s^2 + (\alpha + \hat{\alpha})^2 + (\beta + \hat{\beta})^2 + \mu^2 + \theta^2\right] \tag{1-a}$$

Its time derivative can therefore be written as follows:

$$\dot{v} = s\dot{s} + \dot{\hat{\alpha}}(\alpha + \hat{\alpha}) + \dot{\hat{\beta}}(\beta + \hat{\beta}) + \mu\dot{\mu} + \theta\dot{\theta} \tag{2-a}$$

If we consider a sliding surface governed by the following state equation: $s = \dot{e}_1 + k_s e_1 = e_2 + k_s e_1$, therefore for $\dot{s}$ the following relationship cab be also valid:

$$\dot{s} = \dot{e}_2 + k_s \dot{e}_1 = \dot{e}_2 + k_s e_2 \tag{3-a}$$
$$\dot{s}_2 = f(x,t) + g(x,t)u + d(t) + \Delta F(x,t) - \ddot{x}_d + k_s e_2$$

Substituting Eq. (3-a) into Eq. (2-a), we can write:

$$\dot{v} = s\left[f(x,t) + g(x,t)u + d(t) + \Delta F(x,t) - \ddot{x}_d + k_s e_2\right] + \dot{\hat{\alpha}}(\alpha + \hat{\alpha}) + \dot{\hat{\beta}}(\beta + \hat{\beta}) + \mu\dot{\mu} + \theta\dot{\theta} \tag{4-a}$$

Next, substituting the control law of Eq. (3) and the related relationship of $\dot{\hat{\alpha}}$, $\dot{\hat{\beta}}$, $\dot{\mu}$, and $\dot{\theta}$ into Eq. (4-a), the time derivative of the Lyapunov function $\dot{v}$ can be re-written as:

$$\dot{v} = s\left[-(\hat{\alpha} + \hat{\beta} + \mu)\tanh(\theta s) + d(t) + \Delta F(x,t)\right] - |s|(\hat{\alpha} + \alpha) - |s|(\hat{\beta} + \beta) - p|s||e_1| - q|s||e_1| \tag{5-a}$$

According to the assumed conditions: $|\Delta F(x,t)| \leq \alpha$ and $|d(t)| \leq \beta$, consequently the following conditions can also be verified: $s\Delta F(x,t) \leq |s|\alpha$ and $sd(t) \leq |s|\beta$.

Assuming the abovementioned relationships, the following inequality can be obtained for $\dot{v}$:

$$\dot{v} \le -\left(\hat{\alpha} + \hat{\beta} + \mu\right) s \tanh(\theta s) + |s|\beta + |s|\alpha - |s|\left(\hat{\alpha} + \alpha\right) - |s|\left(\hat{\beta} + \beta\right) - \mu p |s||e_1| - \theta q |s||e_1| \qquad \text{(6-a)}$$

$$\dot{v} \le -\left(\hat{\alpha} + \hat{\beta} + \mu\right) s \tanh(\theta s) - |s|\left(\hat{\alpha} + \hat{\beta} + \mu p |e_1| + \theta q |e_1|\right)$$

Knowing that: $s \tanh(\theta s) = |s||\tanh(\theta s)|$ [41], $\dot{v}$ can be finally re-written as follows:

$$\dot{v} \le -|s|\left\{\left(\hat{\alpha} + \hat{\beta}\right)\left[|\tanh(\theta s)| + 1\right] + \mu\left[|\tanh(\theta s)| + p|e_1|\right] + \theta q |e_1|\right\} \qquad \text{(7-a)}$$

The term inside of brackets "{ }" represents a positive number, and subsequently the condition $\dot{v} \le -|s|\{\eta\}$ for the presented controller is therefore guaranteed, for which η represents a positive number.

References

1.	Khan, F., J. Lu, and Y. Zhu, *Experimental investigation of actuation in a micromachined electrically floating tunable capacitor.* Microelectronic Engineering, 2019. **213**: p. 31-34.
2.	Dai, H.-Y. and L. Li, *Wideband tunable high common-mode suppression filter based on varactor-loaded slotted ground.* Progress In Electromagnetics Research, 2018. **77**: p. 73-80.
3.	Galisultanov, A., et al., *Contactless four-terminal MEMS variable capacitor for capacitive adiabatic logic.* Smart Materials and Structures, 2018. **27**(8): p. 084001.
4.	Gong, Z., et al., *Optimization of a MEMS variable capacitor with high linearity and large tuning ratio.* Microsystem Technologies, 2018. **24**(7): p. 3169-3178.
5.	Teymoori, M.M. and J.M. Ahangarkolaei, *A tunable capacitor based on MEMS technology for RF applications.* Engineering, Technology & Applied Science Research, 2016. **6**(3): p. 982-986.
6.	Jamil, A., T.S. Kalkur, and N. Cramer, *Tunable ferroelectric capacitor-based voltage-controlled oscillator.* IEEE transactions on ultrasonics, ferroelectrics, and frequency control, 2007. **54**(2): p. 222-226.
7.	Jin, J., et al., *A wideband voltage-controlled oscillator with gain linearized varactor bank.* IEEE Transactions on Components, Packaging and Manufacturing Technology, 2014. **4**(5): p. 905-910.
8.	Komatsu, T., et al., *Tunable radio-frequency filters using acoustic wave resonators and variable capacitors.* Japanese Journal of Applied Physics, 2010. **49**(7S): p. 07HD24.
9.	Konno, A., et al., *Tunable surface acoustic wave filter using integrated micro-electro-mechanical-system based varactors made of electroplated gold.* Japanese Journal of Applied Physics, 2013. **52**(7S): p. 07HD13.
10.	Vitale, W.A., et al., *Electrothermal actuation of vanadium dioxide for tunable capacitors and microwave filters with integrated microheaters.* Sensors and Actuators A: Physical, 2016. **241**: p. 245-253.
11.	Kuhn, W., et al., *A microtransceiver for UHF proximity links including Mars surface-to-orbit applications.* Proceedings of the IEEE, 2007. **95**(10): p. 2019-2044.
12.	Afrang, S., et al., *A new MEMS based variable capacitor with wide tunability, high linearity and low actuation voltage.* 2015. **46**(2): p. 191-197.
13.	Mobki, H., et al., *Design, simulation and bifurcation analysis of a novel micromachined tunable capacitor with extended tunability.* 2014. **38**(1): p. 15-29.

14. Nabovati, H., et al., *Design and Simulation of an Oblique Suspender MEMS Variable Capacitor.* 2006.

15. Li, L., et al. *Symmetric toggle structured MEMS linear variable capacitor with large tunning ratio.* in *The 8th Annual IEEE International Conference on Nano/Micro Engineered and Molecular Systems.* 2013. IEEE.

16. Oz, A., *CMOS/BiCMOS self-assembling and electrothermal microactuators for tunable capacitors.* 2003, CARNEGIE-MELLON UNIV PITTSBURGH PA DEPT OF ELECTRICAL AND COMPUTER ENGINEERING.

17. Choi, S., et al. *A tunable capacitor using an immiscible bifluidic dielectric.* in *2004 IEEE MTT-S International Microwave Symposium Digest (IEEE Cat. No. 04CH37535).* 2004. IEEE.

18. Deng, J., Y. Hao, and S. Liu, *Modeling and control of threshold voltage based on pull-in characteristic for micro self-locked switch.* Solid-State Electronics, 2017. **135**: p. 85-93.

19. Deng, Z., et al., *Design and analysis a novel RF MEMS switched capacitor for low pull-in voltage application.* Microsystem Technologies, 2016. **22**(8): p. 2141-2149.

20. Barzegar, S., H. Mirzajani, and H.B.J.W.P.C. Ghavifekr, *A new linearly tunable RF MEMS varactor with latching mechanism for low voltage and low power reconfigurable networks.* 2015. **83**(3): p. 2249-2265.

21. Akhtar, A., et al. *Design and Simulation of MEMS based Varactor with High Tunability for Digital Communication Systems.* in *2018 IEEE 9th Annual Information Technology, Electronics and Mobile Communication Conference (IEMCON).* 2018. IEEE.

22. Ramli, N.A., et al., *Design, simulation and analysis of a digital RF MEMS varactor using thick SU-8 polymer.* 2018. **24**(1): p. 473-482.

23. Mobki, H., et al., *On the tunability of a MEMS based variable capacitor with a novel structure.* 2011. **17**(9): p. 1447.

24. Afrang, S. and N.J.M.T. Nematkhah, *A new MEMS based variable capacitor using electrostatic vertical comb drive actuator and auxiliary cantilever beams.* 2019: p. 1-11.

25. Pagazani, J., et al., *A new design for rotational, tunable wideband RF MEMS capacitors.* 2011. **17**(4): p. 513-522.

26. Martowicz, A., I. Stanciu, and T. Uhl, *Uncertainty analysis for dynamic properties of MEMS resonator supported by fuzzy arithmetics.* The International Journal of Multiphysics, 2016. **3**(3).

27. AkhavanAlavi, S., M. Mohammadimehr, and S.J.E.J.o.M.-A.S. Edjtahed, *Active control of micro Reddy beam integrated with functionally graded nanocomposite sensor and actuator based on linear quadratic regulator method.* 2019. **74**: p. 449-461.

28. Mobki, H., et al., *Multi input versus single input sliding mode for closed-loop control of capacitive micro structures.* 2019. **1**(7): p. 676.

29. Mazumder, J., L. Song, and C. Wang, *In-situ identification and control of microstructures produced by phase transformation of a material.* 2019, Google Patents.

30. Mohammadi, M., et al., *Nonlinear robust adaptive multi-modal vibration control of bi-electrode micro-switch with constraints on the input.* 2017. **8**(9): p. 263.

31. Wang, Y., et al., *Identification of contact bouncing vibrations using TFC active slider and adaptive fuzzy control for advanced active slider design.* 2014. **20**(8-9): p. 1705-1713.

32. Xu, B. and P. Zhang, *Minimal-learning-parameter technique based adaptive neural sliding mode control of MEMS gyroscope.* Complexity, 2017. **2017**.

33. Rahmani, M., *MEMS gyroscope control using a novel compound robust control.* ISA transactions, 2018. **72**: p. 37-43.

34. Hashtarkhani, B., M.J.S.I.T.D. Aghababa, Computer Science, and E. Engineering, *Introducing a new sliding manifold applied for control of uncertain nonlinear brushless DC and permanent magnet synchronous motors.* 2013. **20**(6): p. 2073.

35.   Aghababa, M.P.J.I.A.T.o.M., *Sliding-mode control composite with disturbance observer for tracking control of mismatched uncertain nDOF nonlinear systems.* 2017. **23**(1): p. 482-490.

36.   Aghababa, M.P.J.I.T.o.S., Man, and C. Systems, *Stabilization of canonical systems via adaptive chattering free sliding modes with no singularity problems.* 2018.

37.   Rahmani, M., et al., *Optimal novel super-twisting PID sliding mode control of a MEMS gyroscope based on multi-objective bat algorithm.* 2018. **24**(6): p. 2835-2846.

38.   Rahmani, M. and M.H.J.M.T. Rahman, *A novel compound fast fractional integral sliding mode control and adaptive PI control of a MEMS gyroscope.* 2019: p. 1-7.

39.   Rajaei, A., et al., *Integral sliding mode control for nonlinear damped model of arch microbeams.* 2019. **25**(1): p. 57-68.

40.   Khalili, A.A., Z. Mohamed, and M.A.M.J.M.T. Basri, *Enhanced backstepping sliding mode controller for motion tracking of a nonlinear 2-DOF piezo-actuated micromanipulation system.* 2019: p. 1-13.

41.   Aghababa, M.P., M.E.J.A.M. Akbari, and Computation, *A chattering-free robust adaptive sliding mode controller for synchronization of two different chaotic systems with unknown uncertainties and external disturbances.* 2012. **218**(9): p. 5757-5768.

42.   Slotine, J.-J.E. and W. Li, *Applied nonlinear control*. Vol. 199. 1991: Prentice hall Englewood Cliffs, NJ.

43.   Mobki, H., M. Sadeghi, and G.J.I.J.o.E. Rezazadeh, *Application of Thau observer for fault detection of micro parallel plate capacitor subjected to nonlinear electrostatic force.* 2015. **28**(2): p. 270-276.

44.   Hailu, Z., *High quality factor RF MEMS tunable capacitor.* Microsystem Technologies, 2017. **23**(8): p. 3719-3730.

45.   Kim, J., H. Cho, and J. Park. *A high performance and ultra wide tuned capacitor using netted membrane structure for reconfigurable RF systems*. in *2017 IEEE 30th International Conference on Micro Electro Mechanical Systems (MEMS)*. 2017. IEEE.

46.   Afrang, S., et al., *A new MEMS based variable capacitor with wide tunability, high linearity and low actuation voltage.* Microelectronics Journal, 2015. **46**(2): p. 191-197.

47.   Mobki, H., et al., *Design, simulation and bifurcation analysis of a novel micromachined tunable capacitor with extended tunability.* Transactions of the Canadian Society for Mechanical Engineering, 2014. **38**(1): p. 15-29.

48.   Shavezipur, M., et al., *Linearization and tunability improvement of MEMS capacitors using flexible electrodes and nonlinear structural stiffness.* Journal of Micromechanics and Microengineering, 2012. **22**(2): p. 025022.

49.   Mobki, H., et al., *On the tunability of a MEMS based variable capacitor with a novel structure.* Microsystem technologies, 2011. **17**(9): p. 1447.

50.   Shavezipur, M., et al., *Development of a triangular-plate MEMS tunable capacitor with linear capacitance–voltage response.* Microelectronic Engineering, 2010. **87**(9): p. 1721-1727.